Untangling ciliary access and enrichment of two rhodopsin-like receptors using quantitative fluorescence microscopy reveals cell-specific sorting pathways

Ivayla I. Geneva[a,b], Han Yen Tan[a], and Peter D. Calvert[a,b,c,*]
[a]Center for Vision Research, Department of Ophthalmology, [b]Department of Biochemistry and Molecular Biology, and [c]Department of Neuroscience and Physiology, State University of New York Upstate Medical University, Syracuse, NY 13210

ABSTRACT **Resolution limitations of optical systems are major obstacles for determining whether proteins are enriched within cell compartments. Here we use an approach to determine the degree of membrane protein ciliary enrichment that quantitatively accounts for the differences in sampling of the ciliary and apical membranes inherent to confocal microscopes. Theory shows that cilia will appear more than threefold brighter than the surrounding apical membrane when the densities of fluorescently labeled proteins are the same, thus providing a benchmark for ciliary enrichment. Using this benchmark, we examined the ciliary enrichment signals of two G protein–coupled receptors (GPCRs)—the somatostatin receptor 3 and rhodopsin. Remarkably, we found that the C-terminal VxPx motif, required for efficient enrichment of rhodopsin within rod photoreceptor sensory cilia, inhibited enrichment of the somatostatin receptor in primary cilia. Similarly, VxPx inhibited primary cilium enrichment of a chimera of rhodopsin and somatostatin receptor 3, where the dual Ax(S/A)xQ ciliary targeting motifs within the third intracellular loop of the somatostatin receptor replaced the third intracellular loop of rhodopsin. Rhodopsin was depleted from primary cilia but gained access, without being enriched, with the dual Ax(S/A)xQ motifs. Ciliary enrichment of these GPCRs thus operates via distinct mechanisms in different cells.**

Monitoring Editor
Reid Gilmore
University of Massachusetts

Received: Jul 27, 2016
Revised: Dec 5, 2016
Accepted: Dec 9, 2016

INTRODUCTION

Cilia serve as sensory organelles that transduce physical and chemical signals found in the extracellular environment (Pazour and Witman, 2003; Marshall and Nonaka, 2006; Singla and Reiter, 2006). To facilitate this role, signal transduction cascade proteins are enriched within cilia via transport machinery that is believed to use sequences of amino acids to direct them to the ciliary compartment, often referred to as ciliary targeting sequences (CTSs; Godsel and Engman, 1999; Tai *et al.*, 1999; Dwyer *et al.*, 2001; Corbit *et al.*, 2005; Jenkins *et al.*, 2006; Mazelova *et al.*, 2009; Emmer *et al.*, 2010; Follit *et al.*, 2010; Wang and Deretic, 2014). One such motif, C-terminal VxPx (Deretic *et al.*, 1998; Tam *et al.*, 2000), was identified as being essential for efficient enrichment of the G protein–coupled receptor (GPCR) rhodopsin (Rho) in vertebrate rod photoreceptor sensory cilia, the rod outer segments (ROS). Similar motifs containing a VxP sequence were subsequently identified in a number of ROS-enriched proteins, as well as in several proteins that are enriched in primary cilia. The olfactory cyclic nucleotide–gated channel subunit B1b (CNGB1b) contains a C-terminal RVxP sequence that was reported to be necessary for ciliary enrichment of the heterotetrameric channel (Jenkins *et al.*, 2006). The ciliary cation channel polycystin-2 (PC-2), one of two proteins in which mutations cause autosomal dominant polycystic kidney disease (ADPKD), contains an RVxP motif near its N-terminus that appears to be required for ciliary localization in the absence of polycystin-1 (PC-1; Geng *et al.*, 2006). PC-1, the other ADPKD protein involved in cell adhesion

This article was published online ahead of print in MBoC in Press (http://www.molbiolcell.org/cgi/doi/10.1091/mbc.E16-07-0549) on December 14, 2016.
*Address correspondence to: Peter D. Calvert (calvertp@upstate.edu).
Abbreviations used: CTS, ciliary targeting sequence; Rho, rhodopsin; SR3, somatostatin receptor type 3.

before ciliogenesis and in regulating the PC-2 channel once cilia elaborate, contains its own C-terminal RVxP motif required for ciliary enrichment (Ward *et al.*, 2011). More recently, a VxP motif near the N-terminal of the Na^+, K^+ ATPase (NKA) α4 subunit was found to be the likely motif for flagellar enrichment of NKA, the cation transporter responsible for maintaining the electrochemical ion gradient across the plasma membrane in sperm (Laird *et al.*, 2015). The role of VxPx in targeting/sorting of proteins to ciliary compartments does not appear to be restricted to intrinsic membrane proteins: a peripheral membrane protein, photoreceptor-specific retinal dehydrogenase (prRDH), contains a (V/I)xPx sequence at its extreme C-terminus that was reported to be required for enrichment within photoreceptor OSs (Luo *et al.*, 2004).

The VxPx motif is not, however, the sole ciliary enrichment signal. Odorant GPCRs in *Caenorhabditis elegans* do not possess a VxPx motif, apparently relying instead on an FR sequence just after the seventh transmembrane helix for ciliary localization in olfactory neurons (Dwyer *et al.*, 2001). The somatostatin receptor type 3 (SR3) and the serotonin receptor type 6 (Htr6) are cilium enriched, but neither possesses the VxPx motif. These GPCRs appear to rely on two cilium-targeting consensus sequences, Ax(S/A)xQ, within their third intracellular (i3) loops for ciliary enrichment (Berbari *et al.*, 2008). Of interest, Rho and several other GPCRs, including cone opsins, olfactory receptors, α-2A adrenergic receptor, melanin-concentrating hormone receptor 1 (Mchr1), muscarinic acetyl choline receptor M5, and chemokine orphan receptor 1, also possesses a single Ax(S/A)xQ consensus sequence within their i3 loops (Berbari *et al.*, 2008). Although Mchr1 was shown to enrich in primary cilia of inner medullary collecting duct (IMCD) cells, it is unclear what role, if any, the single Ax(S/A)xQ sequence plays in enrichment of opsins within ROS or in ciliary enrichment of the other GPCRs that possess it. Adding to the complexity of the ciliary-targeting motif story, the serotonin receptor type 7 (Htr7) contains the VxP motif in its i3 loop but is not cilium enriched, suggesting that the motif is not sufficient to impart ciliary targeting on its own. The lack of ciliary targeting of Htr7 by the i3-loop VxP motif is not due to some other ciliary exclusion signal within Htr7, however, because replacing the VxP with a stretch of the i3 loop of SR3 that contains the dual Ax(S/A)xQ motifs results in apparent ciliary enrichment of the chimeric GPCR (Berbari *et al.*, 2008).

The multiple ciliary-targeting motifs and the variable effect of the VxPx motif on ciliary enrichment indicate that ciliary targeting of rhodopsin-like GPCRs involves multiple, perhaps competitive mechanisms. Assessing membrane protein enrichment within cilia, however, is significantly hampered by the geometry of the cell structures being examined and the optical properties of the confocal or epifluorescence microscopes typically used to determine enrichment. Here we examined the ciliary enrichment activity of i3-loop Ax(S/A)xQ and C-terminal VxPx motifs within two GPCRs—SR3 and Rho—that are enriched in two different ciliated cells, using a quantitative, live-cell ciliary enrichment assay. Remarkably, we find that the C-terminal VxPx motif that is required for ROS enrichment of rhodopsin disrupts ciliary enrichment of SR3 and Rho-SR3 chimeras expressed in IMCD3 cells.

RESULTS

Rho and SR3, seven-transmembrane-spanning GPCRs belonging to the rhodopsin-like family, are shown schematically in Figure 1, A and B. Despite the fact that SR3 is highly enriched in primary cilia of epithelial cells and Rho is highly enriched in ROS, the sequences of these GPCRs differ significantly in their putative CTSs. SR3 lacks the VxPx motif that is required for Rho enrichment in rod OSs (Figure 1C). Instead, it contains a pair of Ax(S/A)xQ motifs in its i3 loop that appear to be required for ciliary enrichment in IMCD3 cells (Figure 1, C and D). Rho contains the C-terminal VxPx motif and possesses a single Ax(S/A)xQ in its i3 loop (Figure 1, C and D). To examine the effect of VxPx and Ax(S/A)xQ on ciliary enrichment in IMCD cells, we generated a range of chimeric proteins labeled with either enhanced green fluorescent protein (EGFP) or mKate2 (Figure 1E), expressed them in IMCD cells under the cytomegalovirus (CMV) promoter, and examined their subcellular distribution using live-cell three-dimensional (3D) confocal microscopy.

Expression patterns of SR3 and Rho in ciliated IMCD3 cells differ dramatically

The 3D scanning confocal images of IMCD3 cells expressing SR3-GFP or Rho-GFP show that the distributions of these GPCRs are highly divergent (Figure 2). Fluorescence in SR3-GFP–expressing cells is brightest in the ciliary compartment, with variable but lower fluorescence levels in other cell structures (Figure 2A; see also later discussion of Figures 6E and 7C). In contrast, fluorescence in Rho-GFP–expressing cells was widely dispersed, with fluorescence appearing throughout the cytoplasm and membrane structures often in foci of varying size (Figure 2B, left). The GFP fluorescence signal was rarely visible as a distinct ciliary structure. Therefore, to confirm that cilia were present and identify their location in Rho-GFP–expressing cells, we coexpressed SR3-mKate2 (Figure 2B, right, red). Despite identifying the location of the cilium in this way, it remained difficult or impossible to identify ciliary structures by visual inspection of the GFP channel images.

The inability to detect a ciliary structure in cells expressing Rho-GFP was somewhat surprising, given that Rho contains an Ax(S/A)xQ motif, which was implicated in ciliary enrichment of SR3 and Htr6 (Berbari *et al.*, 2008), as well as the VxPx motif, which is the putative Rho ROS targeting sequence. However, Berbari *et al.* (2008) showed that SR3 and Htr6 possessed two Ax(S/A)xQ motifs in their i3 loops and that both were needed to obtain the greatest ciliary enrichment. In addition, their study showed that introducing the i3 loop of SR3 into SR5, a somatostatin receptor variant that does not normally enrich in cilia, as well as into Htr7, resulted in ciliary enrichment of the chimeras, suggesting that the pair of Ax(S/A)xQ motifs were necessary to confer ciliary enrichment. We thus wondered whether replacing the i3 loop of rhodopsin with that of SR3 would result in ciliary enrichment. To test this idea, we generated a chimera between Rho and SR3, replacing Rho-GFP amino acids (aa) 232–248 with SR3 aa 236–258 (Rho-i3S-GFP; Figure 1). The distribution of Rho-i3S-GFP in ciliated IMCD3 cells was quite different from the distribution of Rho-GFP (Figure 2C). Most notably, cilia were easily detected in confocal images; SR3-mKate2 was not required for detection by eye. However, the distribution was also different from that of SR3-GFP. EGFP signal in Rho-i3S-GFP–expressing cells seemed greater in other cell structures and membranes than the EGFP signal in SR3-GFP–expressing cells (Figure 2; see also later discussion of Figures 4A and 7D). Thus, whereas replacing the i3 loop of rhodopsin with that of SR3 seemed to result in ciliary access of the chimeric protein, it was not clear whether it resulted in ciliary enrichment relative to other cell structures. We therefore sought a way to quantify ciliary enrichment in living cells to differentiate between mere access and true enrichment.

Quantification of GPCR ciliary enrichment: establishing an enrichment threshold

We reasoned that the most relevant definition for ciliary enrichment of a GPCR is a higher spatial density of the GPCRs on the

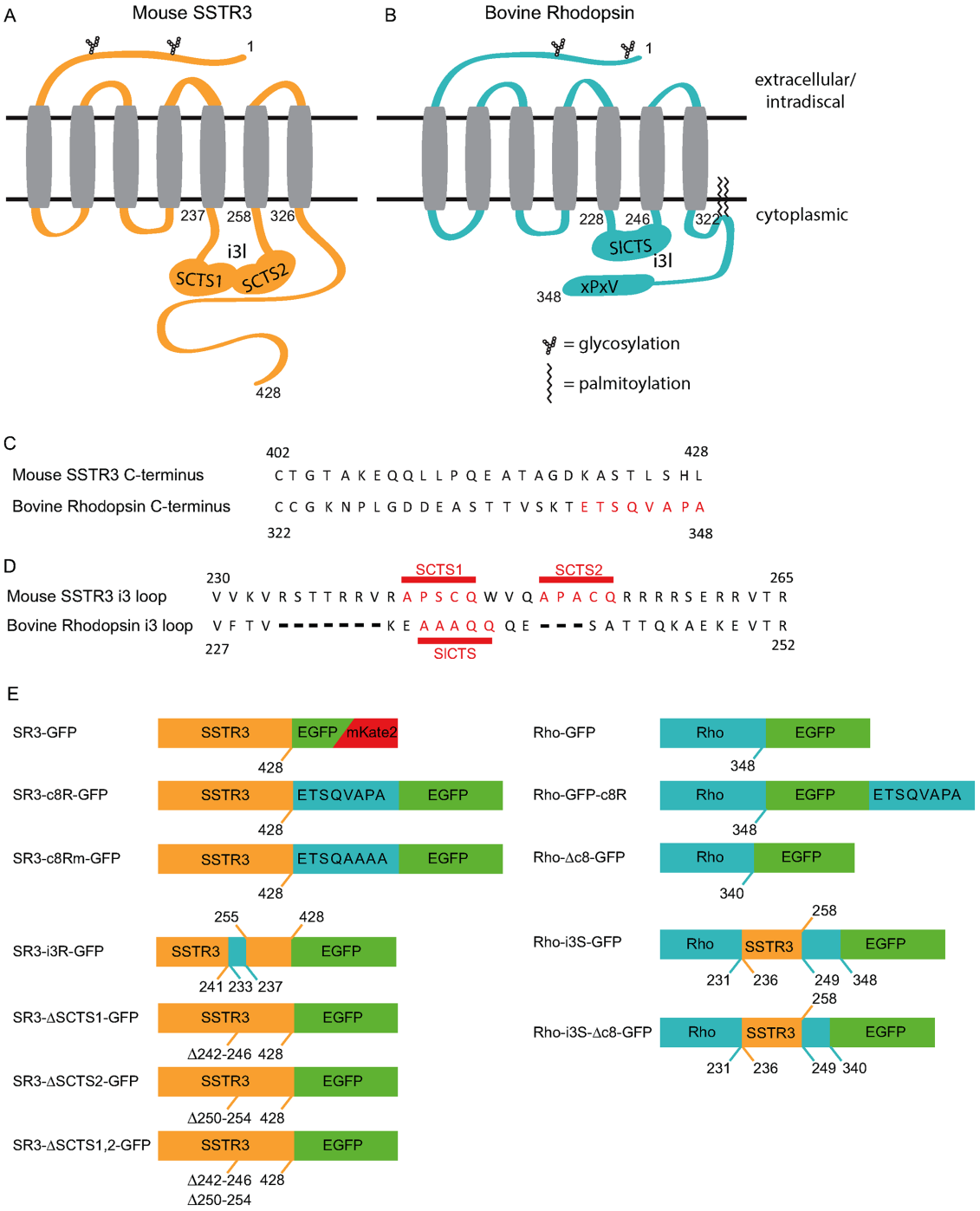

FIGURE 1: Location and structure of SR3 and bovine Rho ciliary-targeting sequences and the constructs used to probe their activity. (A) Structure of SR3, highlighting the dual ciliary-targeting sequences within the third intracellular loop (i3l). SCTS, SR3 ciliary-targeting sequence. (B) Structure of bovine Rho, highlighting the i3l SR3-like ciliary-targeting sequence (SlCTS) and the c-terminal VxPx motif. (C) Sequence comparison of the C-termini of SR3 and Rho. (D) Sequence comparison of the third intracellular loops of SR3 and Rho. (E) Constructs used in this study.

cilium membrane relative to that on the apical membrane. These two membranes are contiguous, albeit with a membrane protein diffusion barrier at or near the cilium base (Hu *et al.*, 2010). Although the GPCRs may be found in other membrane structures within the cell or on the basolateral plasma membrane, a difference in density between the apical membrane and ciliary membrane would directly show active maintenance of a local concentration gradient.

To quantify the relative density of GPCRs within these membrane compartments, one must take into account how the imaging system samples the membranes. We thus modeled the sampling of the ciliary and apical membranes by the microscope point spread function (*psf*; Figure 3). The ciliary membrane can be approximated as a right circular cylinder with diameter ~300 nm and variable length up to ~10 μm (Figure 3A). Cilia that were imaged and analyzed were generally lying flat against the apical membrane surface of the cells and

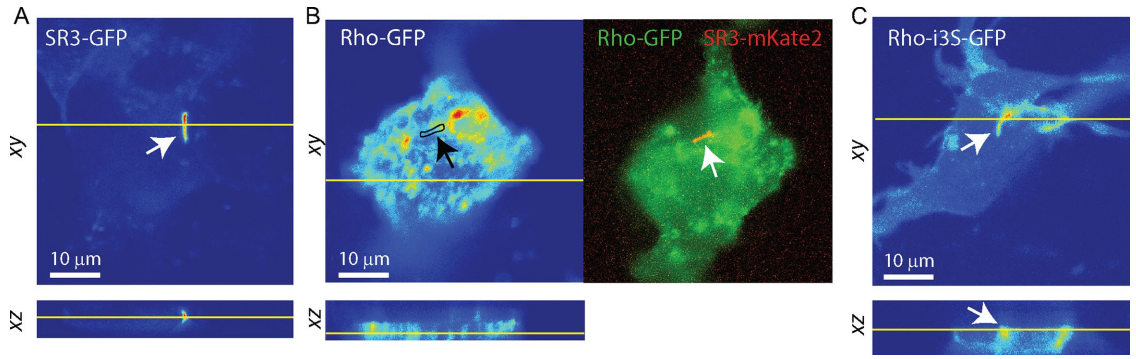

FIGURE 2: SR3 and Rho distributions differ greatly within ciliated IMCD3 cells. (A) Fluorescence profiles of an SR3-GFP–expressing cell in *xy* and *xz* appear mostly in the cilium (arrow). (B) The fluorescence in the Rho-GFP–expressing cell is broadly distributed, with focal hot spots. Location of the cilium (black outline and arrow) was ascertained from the coexpressed SR3-mKate2 (right). The cilium was not readily detectable in the EGFP channel in virtually all cells examined ($n = 11$). (C) Replacing the i3l of Rho with the i3l of SR3 resulted in cilia (white arrow) that were readily detectable, although other structures appeared brighter than in SR3-GFP–expressing cells.

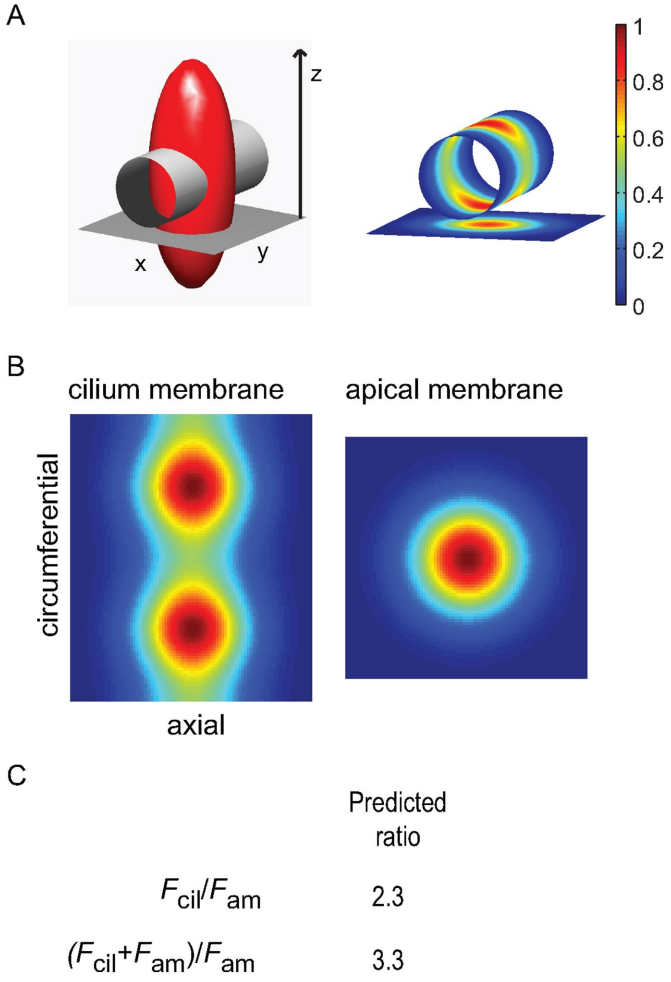

FIGURE 3: Theoretical calculation of the threshold for ciliary enrichment. (A) Left, isointensity surface of the excitation *psf* (shown as $(1/e)I_{max}$; red ellipsoid) intersecting with a right circular cylinder with diameter 300 nm and length 1 μm, which represent the average cilium geometry, and a planar surface 1 μm square orthogonal to the *z*-axis (the optical axis, or axis of light propagation), which represents the apical membrane. Right, projected *psf* intensity profiles at the cylinder (cilium) and planar (apical membrane) surfaces, as obtained by coordinate interpolation. (B) Projected *psf* intensity profiles at the cylinder and planar surfaces shown en face, where the cylinder has been sliced along one side and laid flat. The pixel dimensions of the two surfaces are identical and set by the angular frequency of the cylinder coordinates, thus allowing direct prediction of expected fluorescence intensity ratios between the cilium and apical membranes, assuming uniform density of fluorophore, by finding the quotient of the two-dimensional integration of each profile. (C) Predicted F_{cil}/F_{am} and $(F_{cil}+ F_{am})/F_{am}$ ratios. The latter predicts that the cilium will appear more than threefold brighter than the neighboring apical membrane in raw fluorescence images when the spatial density of fluorophores is identical within the two membrane compartments.

thus were approximately orthogonal to the *z*-axis of the microscope system. Both membranes are on the order of a few nanometers thick, and the GPCRs tether the fluorescent protein labels to a region within a few nanometers of the intracellular leaflet of the membranes. The result of these geometries is that the EGFP-labeled GPCRs are sampled by a subvolume of the *psf* profile for any given acquisition voxel (Figure 3, A and B). Sampling of the ciliary membrane and the apical membrane by the *psf* was thus evaluated by comparing the intersections of the 3D *psf* with a cylinder of 0.3 μm diameter and 1 μm length or a planar apical membrane of 1 μm^2 (Figure 3B). Not surprisingly, this analysis shows that a larger effective area is probed when the *psf* samples the ciliary membrane than when it samples the apical membrane. It is also clear that, when the structures are centered on the *psf*, different regions of the *psf* profile are intersected by the structures: the apical membrane intersects the center, and thus brightest part of the *psf*, whereas the cilium membrane does not.

To quantify the effect of these differences in membrane sampling on estimation of the spatial density of GPCRs, we computed the integral of the element-wise matrix products of the model membranes and the *psf* profile, assuming that both membranes were centered on the *psf* in *z* and that the apical membrane was perpendicular to the optical z-axis. The ratio of the expected fluorescence obtained from the cilium membrane to that obtained from the apical membrane was then found as $F_{cil}/F_{am} = 2.3$ (Figure 3C). This result shows that the cilium fluorescence is expected to be more than twofold brighter than that of the apical membrane when the two membranes have identical densities of GPCRs, that is, in the absence

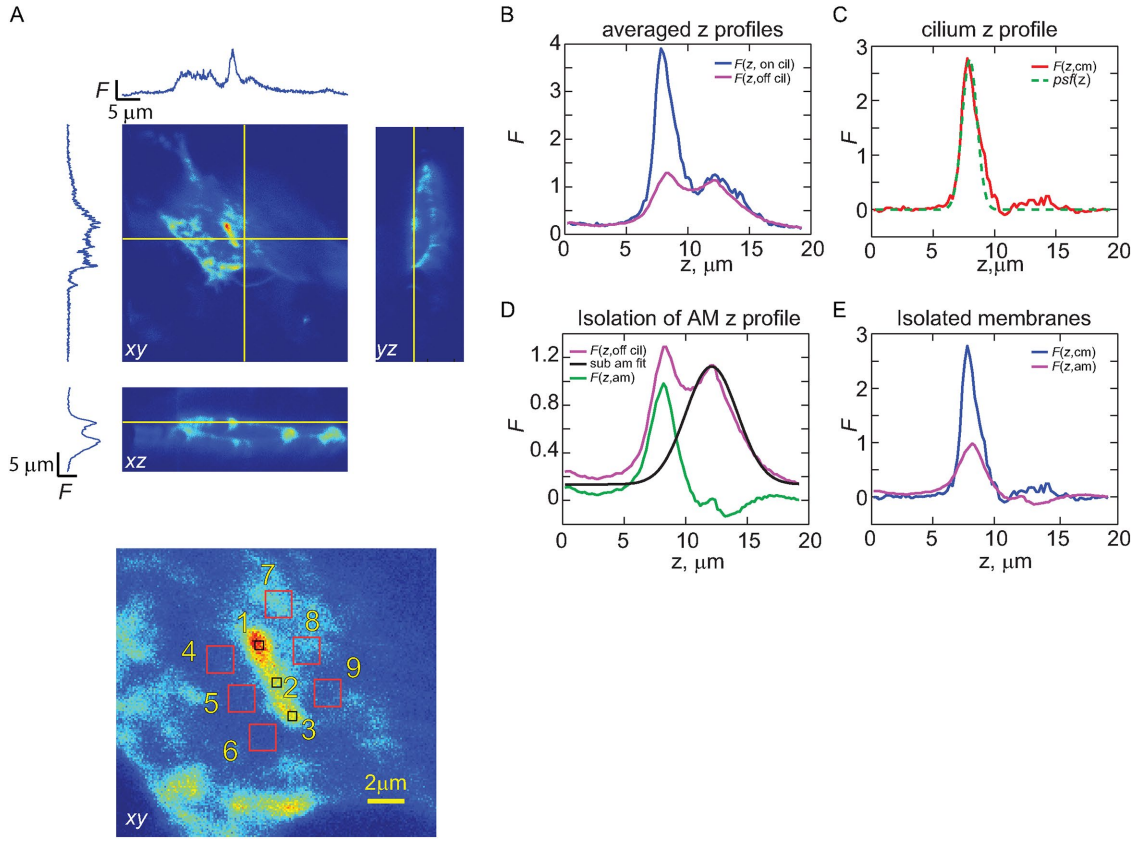

FIGURE 4: Strategy for isolating fluorescence originating from cilia and apical membranes. (A) Representative 3D *z*-stack of an IMCD3 cell expressing an EGFP-tagged GPCR. Yellow lines indicate planes of the displayed *xy*-, *xz*-, and *yz*-images. Bottom, red numbered boxes indicate regions of interest (ROIs) where *z*-profiles, averaged in *xy*, were obtained. (B) For each cell analyzed, three ROIs were selected along the length of the cilium and six were selected from the immediate vicinity of the cilium, and the respective *z*-profiles were averaged to obtain *F*(*z*, on cilium) and *F*(*z*, off cilium). (C) Fluorescence *z*-profile for the cilium alone (F_{cil}), obtained by subtracting *F*(*z*, on cilium) from *F*(*z*, off cilium). Green dashed line represents the scaled *z*-profile of the *psf*. (D) To better isolate the fluorescence emanating from the apical membrane, the region of *F*(*z*, off cilium) profile distal to the apical membrane was fitted with a Gaussian function, and the resulting *z*-profile was subtracted to yield F_{am}. (E) Overlay of the isolated *F*(*z*, cm) and *F*(*z*, am).

of relative enrichment of either membrane. The effect is even more pronounced on visually examining the fluorescence images, that is, when the apical membrane fluorescence is not subtracted from the fluorescence in the region of the cilium. In this case, the cilium fluorescence will appear at least 3.3-fold brighter than the apical membrane, depending on the distance between the membranes, due to the convolution of the two membrane structures by the optical system (Figure 3C).

The $F_{cil}/F_{am} = 2.3$ thus serves as a benchmark for ciliary or apical membrane enrichment, which we term the enrichment threshold (ET). The implication of this result is that the ability to detect cilium fluorescence on the background of apical membrane fluorescence does not, in and of itself, indicate that the labeled membrane protein of interest is cilium enriched. Indeed, the ciliary membrane with lower density of GPCRs relative to the apical membrane can lead to cilium fluorescence that appears brighter than that of the apical membrane.

Quantification of GPCR ciliary enrichment: isolating ciliary membrane and apical membrane GPCR densities

To determine quantitatively the density of the expressed GPCRs within the ciliary membrane relative to their density in the apical membrane, we examined the F_{cil}/F_{am} ratio obtained from 3D confocal scans of IMCD3 cells after ciliary elaboration (Figure 4A). To obtain the average fluorescence of the ciliary membrane, F_{cil}, we averaged the fluorescence *z*-profile, *F*(*z*), from within three regions along the cilium and subtracted fluorescence *z* profiles acquired near those positions (Figure 4, B and C). To isolate F_{am}, we processed the averaged *F*(*z*) profiles acquired near the positions where the ciliary profiles were obtained in order to remove fluorescence signal originating from GPCRs within cytoplasmic membrane structures lying below the apical membrane. Examination of *F*(*z*) in the regions near the cilium showed that the apical membrane could be distinguished from the fluorescence originating from structures below the apical membrane (Figure 4D). F_{am} was thus obtained by fitting the non–apical membrane fluorescence with a Gaussian of arbitrary width, which was then subtracted from the off-cilium *F*(*z*) signal (Figure 4D). The resulting *F*(*z*, cm) and *F*(*z*, am) profiles were then fitted with Gaussians and F_{cil}/F_{am} obtained as the ratio of the Gaussian peaks (F_{pk}; Figure 4E).

Rho-GFP is depleted from IMCD3 primary cilia

The measurement of F_{cil}/F_{am} allows the unequivocal conclusion that SR3-GFP expressed in ciliated IMCD3 cells is highly enriched in

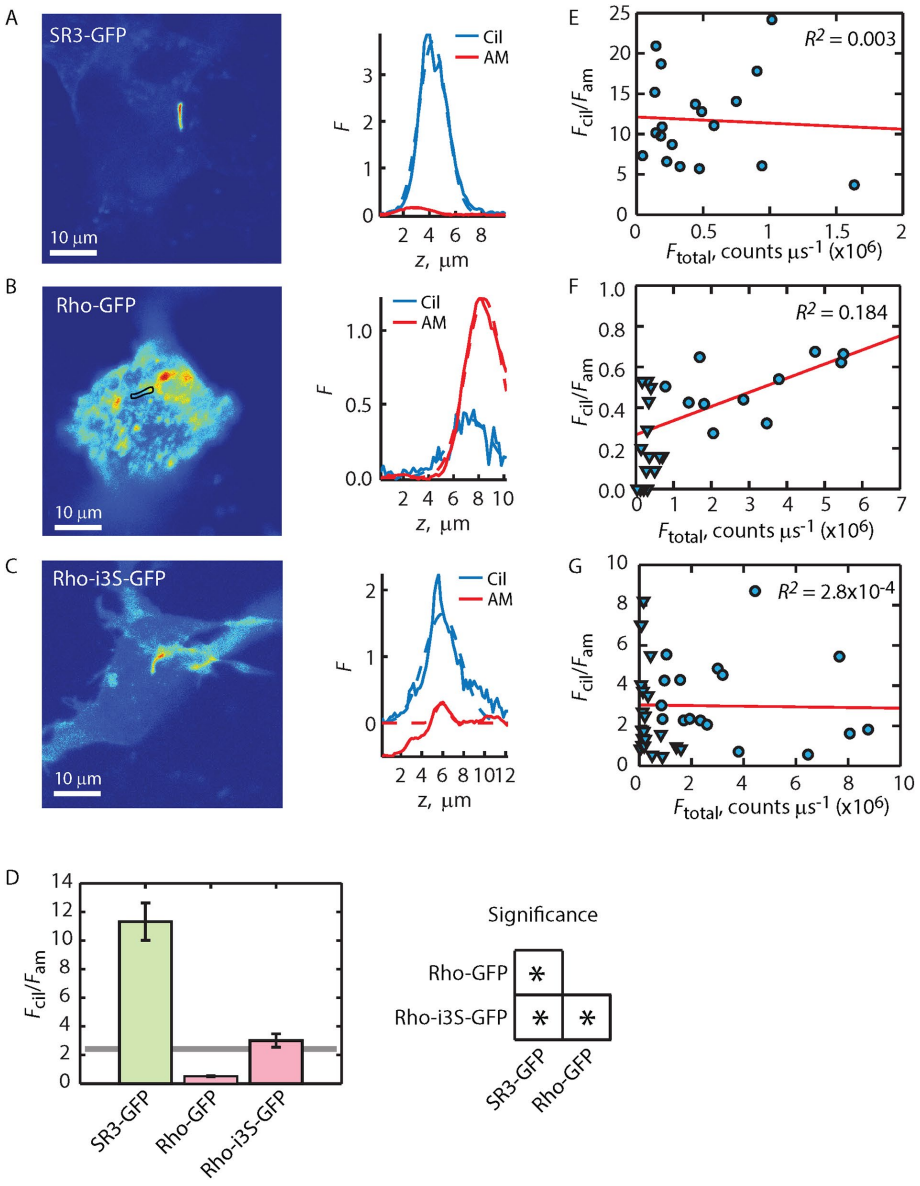

FIGURE 5: Quantification of F_{cil}/F_{am} reveals that Rho-i3S-GFP has access to, but is not enriched within, the ciliary membrane. (A–C) Fluorescence distribution images (left) and F_{cil} and F_{am} *z*-profiles (right) for three GPCR constructs. Solid lines represent the *z*-profiles; dashed lines represent Gaussian fittings of the profiles. (D) Averaged F_{cil}/F_{am} ratios obtained from the ratios of Gaussian fitting peaks (left). Error bars represent SEM (*N*'s provided in Table 1). Solid horizontal line is the enrichment threshold (ET). Right, significance tests; asterisks indicate significance with $p < 0.05$ as determined by post hoc analysis (*Materials and Methods*). (E–G) Individual F_{cil}/F_{am} ratios (symbols) plotted as a function of total GPCR expression (note different axis scaling). Solid lines represent linear regressions of the relations. R^2 values are the coefficients of determination and indicate goodness of fit, where $R^2 = 1$ indicates perfect fit (*Materials and Methods*). Triangles in F and G represent results from cells in which the expression levels of the Rh-GFP constructs were deliberately reduced, allowing direct comparison of ciliary enrichment between Rho and SR3 constructs at similar expression levels (see the text for details).

ciliary membranes by on average fivefold (Figure 5, A and D). To the contrary, $F_{cil}/F_{am} << 2.3$ shows that Rho-GFP is depleted from the ciliary membrane compartment relative to the apical membrane (Figure 5, B and D). Previously it was shown that bovine rhodopsin C-terminally labeled with EGFP did not traffic properly to the OS in mouse rods unless the eight C-terminal amino acids of Rho were repeated after the EGFP (Jin *et al.*, 2003). We thus examined the possibility that Rho-GFP trafficking to the ciliary membrane compartment was similarly interrupted and led to an apparent depletion. The Rho-GFP-c8R construct (Figure 1) repeats the eight C-terminal amino acids on the C-terminus of the EGFP label. Expression of Rho-GFP-c8R in IMCD3 cells resulted in an F_{cil}/F_{am} = 1.08 ± 0.23, not significantly different from the value for Rho-GFP (Table 1), and thus addition of a second VxPx at the C-terminus of Rho-GFP did not lead to improved ciliary enrichment. These results suggest that VxPx on Rho does not play a role in ciliary enrichment of Rho (or SR3) in the context of IMCD3 cells.

Given that SR3 and Rho undergo diffusion in both the ciliary and apical membrane compartments (Hu *et al.*, 2010; Trivedi *et al.*, 2012), these results confirm previous conclusions that GPCRs are actively held in steep gradients between the apical membrane and ciliary membrane compartments (Hu *et al.*, 2010). However, the exclusion of Rho-GFP from the ciliary compartment, and thus the enrichment in the apical membrane relative to the ciliary membrane, is a novel observation that shows that the maintenance of steep gradients may occur in either direction.

Rho-i3S-GFP gains ciliary access but is not enriched

We next examined whether the putative ciliary-targeting sequences found in the i3 loops of SR3 would allow Rho enrichment in the ciliary membranes. Expression of Rho-i3S-GFP resulted in cilia that were easily identified by visual inspection (Figure 2C). However, quantification of the F_{cil}/F_{am} ratio was not significantly different from the enrichment threshold value of 2.3, which indicates that Rho-i3S-G is found at approximately equal density on the apical and ciliary membranes (Figure 5, C and D). This result shows that the Ax(S/A)xQ motifs permitted Rho access to the ciliary compartment but did not support enrichment.

A potential caveat to the foregoing conclusion, however, arises when the expression levels of the labeled GPCRs are examined. Rho-GFP and Rho-i3S-GFP are expressed at significantly higher levels, on average, than SR3-GFP (Table 1). Thus it seems plausible that higher expression levels might lead to GPCRs being misdirected to the apical membrane if, for instance, the capacity of the ciliary membrane were exceeded. To examine this possibility, we plotted the F_{cil}/F_{am} ratio as a function of total GPCR expression (Figure 5, E–G). Remarkably, despite careful transfection of the cultured IMCD3 cells with identical concentrations of plasmid DNA, the average expression levels of Rho constructs significantly exceeded that of the SR3-GFP. To examine whether this higher expression was

Construct	*N*(cells)	*N*(expt)	Mean F_{cil}/F_{am}	Mean F_{total} counts/μs (×10^6)	Range F_{total} counts/μs (×10^6)
SR3-GFP	21	5	11.3 ± 1.27	0.36 ± 0.06	4.3
SR3-GFP (no cilia)	11	3	–	1.09 ± 0.18	2.0
SR3-c8R-GFP	10	3	2.07 ± 0.41	1.28 ± 0.19	2.7
SR3-GFP-c8R	36	6	1.87 ± 0.23	2.91 ± 0.41	10.7
SR3-c8Rm-GFP	12	3	5.87 ± 0.65	1.01 ± 0.08	1.2
SR3-i3R-GFP	21	5	3.37 ± 0.55	1.40 ± 0.27	3.7
SR3-ΔSCTS1-GFP	17	5	3.70 ± 0.55	0.89 ± 0.18	2.8
SR3-ΔSCTS2-GFP	14	4	3.01 ± 0.56	2.40 ± 0.36	4.5
SR3-ΔSCTS1,2-GFP	23	6	3.70 ± 0.27	0.50 ± 0.06	0.95
Rho-GFP	11	3	0.50 ± 0.04	3.05 ± 0.48	4.7
Rho-GFP (low expression)	16	3	0.27 ± 0.08	0.31 ± 0.29	0.67
Rho-GFP-c8R	23	5	1.08 ± 0.23	1.43 ± 0.48	10
Rho-Δc8-GFP	12	3	0.64 ± 0.14	0.82 ± 0.22	2.7
Rho-i3S-GFP	20	4	3.01 ± 0.46	3.49 ± 0.65	15
Rho-i3S-GFP (low expression)	21	3	2.75 ± 0.51	0.37 ± 0.10	1.6
Rho-i3S-GFP-c8R	17	4	4.48 ± 0.60	1.45 ± 0.40	7.3
Rho-i3S-Δc8R-GFP	8	3	7.61 ± 1.12	0.66 ± 0.09	0.98
Rho-i3S-Δc4R-GFP	13	3	8.54 ± 0.89	1.80 ± 0.50	5.7

N(cells) is the total number of cells analyzed. *N*(expt) is the number of discrete experiments (i.e., experiments that took place on different days with distinct cell cultures and ciliogenesis induction). Range refers to the highest value minus the lowest value in the data set. Low-expression experiments used lower concentrations of plasmid for transfection (20% of that used in all other experiments).

TABLE 1: Summary of F_{cil}/F_{am} ratios and overall expression levels.

responsible for the lower ciliary enrichment of Rho constructs, we reduced their overall expression level by reducing the concentration of plasmid DNA used to transfect the cells fivefold (Table 1, Rho-GFP [low expression] and Rho-i3S-GFP [low expression]) and selected for low expressers when imaging. This approach resulted in capturing the distributions of Rho constructs expressing on average ~10-fold lower than at the higher transfection concentration used for all other constructs (Table 1), an expression level well within the range of the SR3-GFP constructs. Despite this dramatic reduction in expression level, the F_{cil}/F_{am} ratio of the Rho-GFP constructs did not increase, and the F_{cil}/F_{am} versus F_{total} plot did not show correlation (Figure 5, F and G, inverted triangles, and Table 1). In fact, the ratio for the Rho-GFP low expresser was approximately half that of the high expresser, a difference that was statistically significant.

The depletion of Rho-GFP and the failure of enrichment of Rho-i3S-GFP suggest that certain features of rhodopsin inhibit its transport to and enrichment within ciliary membranes. It is possible that the Ax(S/A)xQ motif within the rhodopsin i3 loop (AAAQQ) does not support ciliary entry. Alternatively, some other rhodopsin sequence might derail transport to the cilium.

Rhodopsin i3 loop does not affect SR3 ciliary access

To test the possibility that the i3 loop of Rho promoted the depletion of Rho-GFP from the ciliary membrane, we generated the reciprocal chimera consisting of SR3 with its i3 loop replaced by the i3 loop of Rho (Figure 1; SR3-i3R-GFP) and expressed it in IMCD3 cells (Figure 6). The fluorescence pattern of SR3-i3R-GFP was qualitatively similar to that of Rho-i3S-GFP, with the cilium readily discernible but with significant fluorescence present in other membrane structures (Figure 6A). The F_{cil}/F_{am} of SR3-i3R-GFP was 3.37 ± 0.55, indicating modest ciliary enrichment. Similar results were obtained when SR3-GFP lacking either (Figure 6, B and C) or both (Figure 6D) of the Ax(S/A)xQ motifs in the i3 loop were deleted. In each of these cases, the average F_{cil}/F_{am} ratios were at or slightly above the 2.3 enrichment threshold but were significantly below the average F_{cil}/F_{am} ratio of SR3-GFP containing the dual Ax(S/A)xQ motifs (Figure 6F). These results are similar to those of Berbari *et al.* (2008). Together, the results presented here show that the Rho Ax(S/A)xQ motif was not responsible for depletion of Rho-GFP from the cilium. Of interest, the results show that, singly, the i3 loop Ax(S/A)xQ motif has no effect on SR3 access to or enrichment within the ciliary compartment. Only the dual Ax(S/A)xQ motif results in significant ciliary enrichment.

The results thus far do not explain why Rho-i3S-GFP, which possesses the dual motif, is not enriched in the cilium. We thus investigated other sequences in Rho that might lead to ciliary depletion. Because VxPx is absent from SR3, we began by investigating the activity of the VxPx motif.

VxPx eliminates both Rho-i3S and SR3 ciliary enrichment

To investigate the effect of the VxPx motif on GPCR enrichment in the ciliary compartment, we generated several constructs that either added VxPx to SR3 or deleted it from Rho (Figure 1). Addition of the eight C-terminal amino acids of Rho to the C-terminus of SR3 produced the SR3-c8R-GFP chimera. Expression of SR3-c8R-GFP in IMCD3 cells resulted in dramatic reduction of the average F_{cil}/F_{am} ratio to just below the enrichment threshold (Figure 7, A and G). Of importance, the average F_{cil}/F_{am} ratio for SR3-c8R-GFP was not

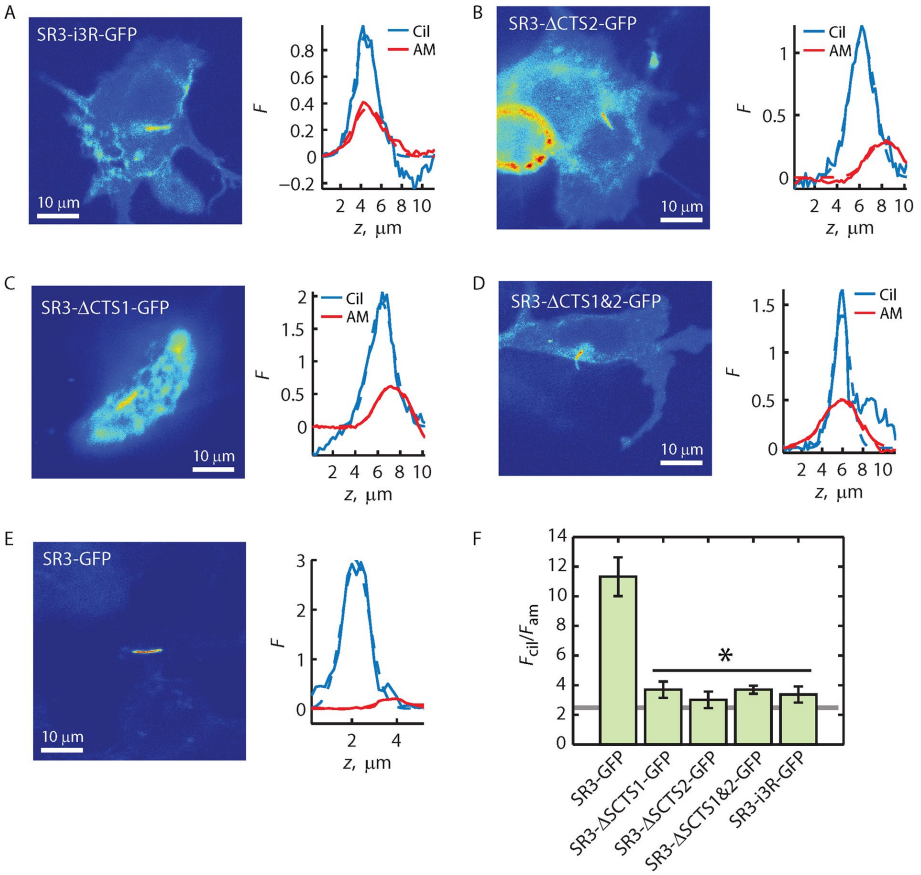

FIGURE 6: Ax(S/A)xQ motif found in the i3 loop of Rho is not a ciliary depletion signal. (A–E) Fluorescence distribution images (left) and F_{cil} and F_{am} *z*-profiles (right) for the indicated GPCR constructs. Solid lines represent the *z*-profiles; dashed lines represent Gaussian fittings of the profiles. (F) Averaged F_{cil}/F_{am} ratios obtained from ratios of the peaks of Gaussian fittings. Error bars represent SEM (*N*'s provided in Table 1). Asterisk indicates that F_{cil}/F_{am} ratio for each construct under the horizontal black line is significantly less than that of SR3-GFP, with $p < 0.05$ as determined by post hoc analysis (*Materials and Methods*). Gray line indicates enrichment threshold.

significantly different from that for Rho-i3S-GFP (Figure 7, D and G). These chimeras contain effectively the same set of trafficking motifs—both contained a VxPx at the C-terminus, as well as the dual i3 loop Ax(S/A)xQ motifs. Mutating the VxPx to AAAA on the SR3 chimera (SR3-c8Rm-GFP) reversed the depletion, resulting in an average F_{cil}/F_{am} ratio of 5.87 ± 2.24 (Figure 7, B and G), a value significantly above those for SR3-c8R-GFP and Rho-i3S-GFP. Note that whereas the F_{cil}/F_{am} ratio of SR3-c8Rm-GFP was a little more than half of the ratio for SR3-GFP, this difference was not significant at the $p = 0.05$ level (Figure 7G).

Remarkably, deletion of the VxPx motif from Rho-i3S-GFP by deleting either the C-terminal four (Rho-i3S-Δc4-GFP) or eight (Rho-i3S-Δc8-GFP) amino acids led to ciliary enrichment (Figure 7, E and G, and Table 1). Rho-i3S-Δc4-GFP produced an average F_{cil}/F_{am} ratio of 8.54 ± 3.21 and Rho-i3S-Δc8-GFP a ratio of 7.61 ± 3.53. These values are significantly greater than the Rho-i3S-GFP F_{cil}/F_{am} ratio but are not significantly below that of SR3-GFP. These results suggest that the VxPx motif acts to disrupt ciliary enrichment of the rhodopsin-like GPCRs. Of interest, deleting the eight C-terminal amino acids that contain the VxPx motif from Rho-GFP (Figure 1; Rho-Δc8-GFP) yielded an average F_{cil}/F_{am} ratio significantly less than that of SR3-i3R-GFP and well below the threshold for enrichment (Table 1). This result indicates that Rho may lack some other important sequence or property that SR3 possesses to allow low-level ciliary access.

Ciliogenesis leads to overall reduction of SR3-GFP expression

Quantitative examination of the expression levels of the various GPCR constructs in the IMCD3 cells revealed an intriguing difference. SR3-GFP underwent a significant down-regulation in expression in the IMCD3 cells upon induction of ciliogenesis. Before ciliogenesis, SR3-GFP expression in transfected IMCD3 cells was higher and more broadly distributed within the apical and basolateral membranes (Figure 8A). Upon induction of ciliogenesis, the overall expression of SR3-GFP decreased more than threefold, and the distribution of SR3-GFP shifted toward enrichment in the cilia (Figure 8B). This result suggested that the enrichment of SR3-GFP in the ciliary compartment involves an increase in retrieval and degradation of SR3 from other membrane compartments upon ciliogenesis. The shift in SR3 away from the apical and basolateral membranes may involve a change in the membrane delivery mechanism to one that favors the cilium compartment or a change in the balance between SR3-GFP delivery to and removal from the apical and basolateral membranes. Either way, the results show that the ciliary enrichment of SR3 upon initiation of ciliogenesis must include significant SR3 degradation.

Expression levels of SR3-GFP chimeras that possessed either the VxPx-containing C-terminal eight amino acids of Rho or the mutated Rho C-terminus, however, were not significantly different than that of SR3-GFP before ciliogenesis (Figure 8B), suggesting that the C-terminus of SR3 may play a critical role in the switching between delivery modes and/or SR3 degradation. In addition, the expression level of SR3-GFP constructs that possessed fewer than two of the Ax(S/A)xQ intracellular loop 3 CTSs was higher than that of the SR3-GFP construct, and the ciliary enrichment was lower (Table 1), suggesting that the CTSs in the third intracellular loop of SR3 may also be involved in the regulation of expression level. To examine whether there was a quantifiable correlation between the overall SR3-GFP construct expression level and the degree of ciliary enrichment, we plotted the average F_{cil}/F_{am} ratio for the various constructs against their average F_{total} value (Figure 9). A clear inverse correlation was apparent that was well fitted with an exponential function (Figure 9A). Despite this clear dependence, the individual constructs showed no such correlation (Figure 9B), indicating that overall expression level alone cannot account for ciliary enrichment or lack thereof. These results, together with the lack of correlation of ciliary enrichment and expression levels of the Rho constructs (Figure 5) and the ciliogenesis-dependent reduction in expression level and ciliary enrichment of SR3-GFP (Figure 8), strongly suggest that whereas ciliary enrichment is significantly correlated with overall expression levels of the GPCRs, this correlation is not due to saturation of the sorting and retrieval mechanisms. Instead, the results indicate that the correlation reflects genuine changes in the balance

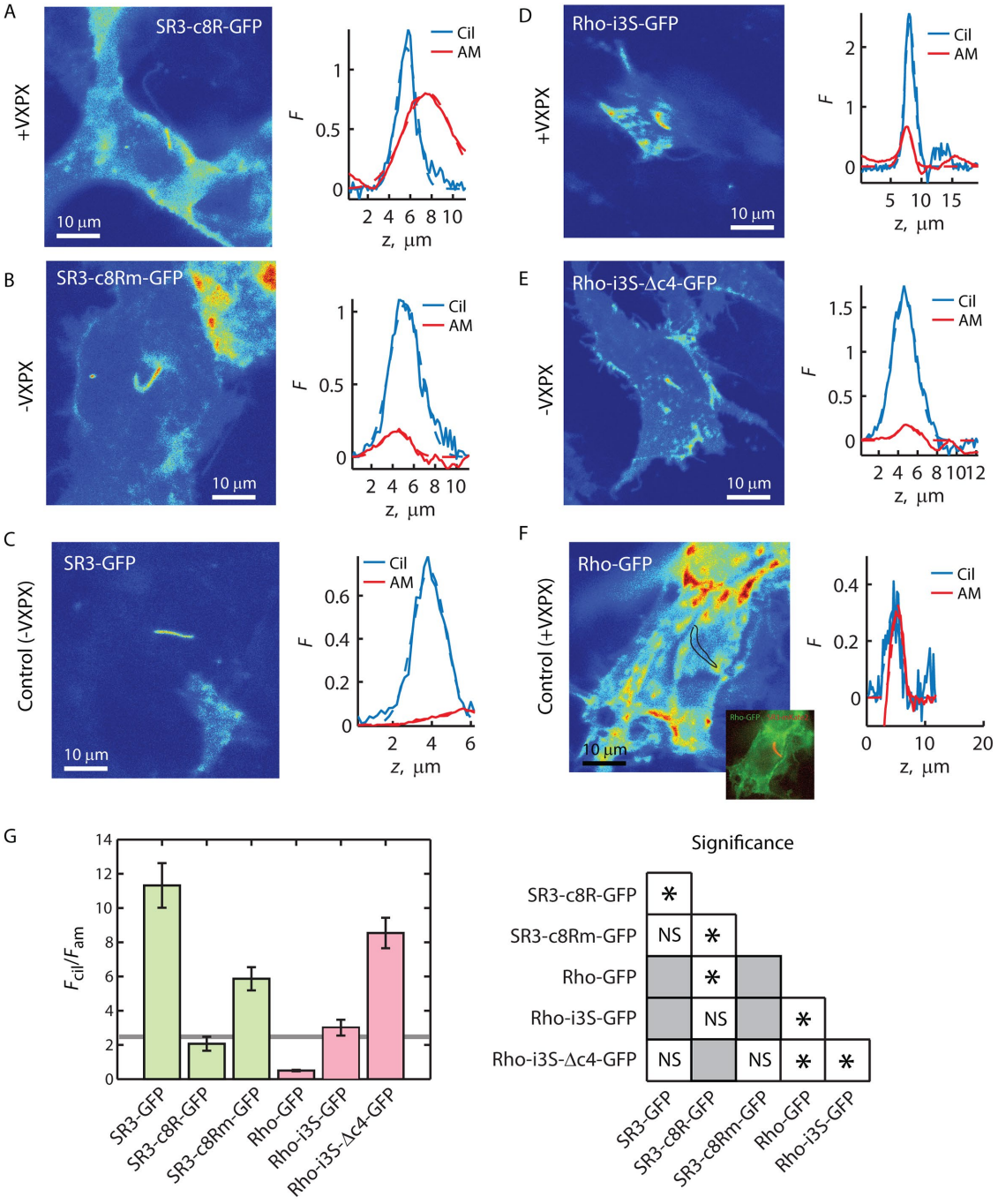

FIGURE 7: C-terminal VxPx reduces ciliary enrichment of SR3 and Rho-i3S. (A–F) Fluorescence distribution images (left) and F_{cil} and F_{am} *z*-profiles (right) for the indicated GPCR constructs. Solid lines represent the *z*-profiles; dashed lines represent Gaussian fittings of the profiles. Inset to F, overlay of Rho-GFP and SR3-mKate2, allowing determination of cilium location (black outline). (G) Averaged F_{cil}/F_{am} ratios obtained from the ratios of Gaussian fitting peaks (left). Error bars represent SEM (*N*'s provided in Table 1). Solid horizontal line is the enrichment threshold. Right, significance tests; asterisks indicate significance with $p < 0.05$ as determined by post hoc analysis (*Materials and Methods*). NS, not significant. Gray squares, not compared.

between delivery and degradation of the GPCRs that result from changes in the interactions of the receptors with the cellular delivery and degradation machinery.

DISCUSSION

Our study underlines the fundamental importance of understanding how optical systems sample specimens at a basic, physical level to the interpretation of experiments aimed at elucidating molecular mechanisms of protein sorting in living cells. Specifically, we show that, in epithelial cells that express fluorescently tagged membrane proteins, observing fluorescence in cilia brighter than the fluorescence in neighboring apical membranes does not necessarily indicate that the cilia are enriched in those proteins. Our approach of quantifying and comparing the density of membrane proteins on

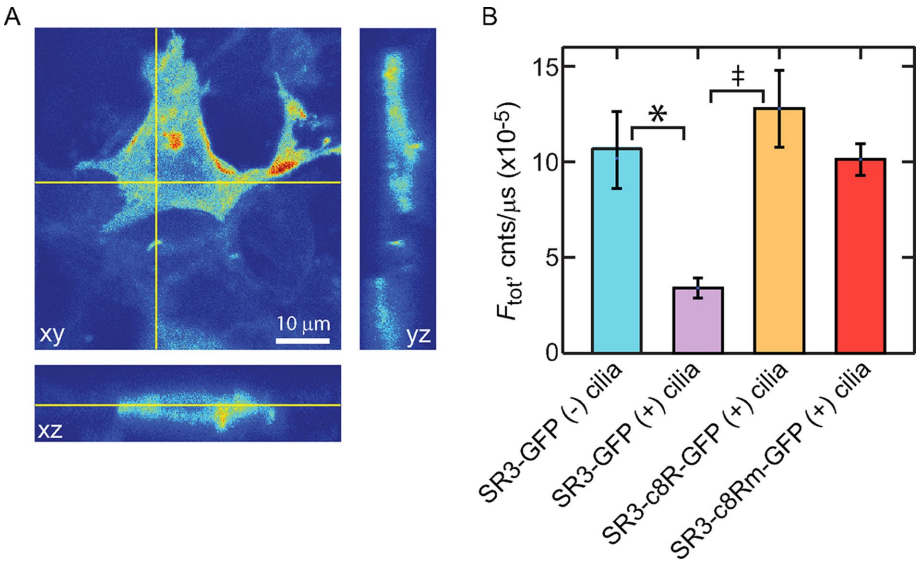

FIGURE 8: Ciliogenesis leads to reduced overall expression of SR3-GFP. (A) A 3D confocal stack of an SR3-GFP–expressing IMCD3 cell before ciliogenesis induction. Fluorescence is found broadly distributed throughout the cell membrane compartments, including the apical and basolateral membranes. (B) Bar chart showing the average total expression levels of indicated constructs. Error bars represent SEM (*N*'s provided in Table 1). Asterisk indicates significance with $p < 0.05$ and double dagger that with $p < 0.01$, as determined by post hoc analysis (*Materials and Methods*).

the ciliary and apical membranes allowed differentiation between mere access of the proteins to cilia and enrichment of the proteins within the ciliary membranes relative to the apical membrane and vice versa. The analysis quantitatively showed that SR3-EGFP is highly enriched in the ciliary membranes, by showing that the ciliary membrane density was fivefold higher than that of the apical membrane. Although this may have seemed obvious from examination of fluorescence micrographs, without the quantitative analysis presented here, it would have remained uncertain. More surprising was the revelation that, despite being present in the cilium, rhodopsin expressed in IMCD3 cells was less dense in cilium membranes than in apical membranes.

IMCD3 cells and photoreceptors use distinct sorting and enrichment strategies for rhodopsin-like GPCRs destined for the ciliary compartment

A number of studies implicated the C-terminal VxPx motif in post-Golgi Rho sorting using cell-free systems or reporter constructs transgenically expressed in photoreceptors (Deretic and Papermaster, 1991; Deretic *et al.*, 1998; Deretic, 2006; Deretic and Wang, 2012; Tam *et al.*, 2000). Deleted or mutated VxPx motifs resulted in significant but incomplete shift in Rho distribution toward the photoreceptor inner segment, perinuclear region, and presynaptic spherule when expressed in rho$^{+/-}$ mouse or *Xenopus* rods (Concepcion *et al.*, 2002; Concepcion and Chen, 2010; Lodowski *et al.*, 2013). Complete mislocalization of mutant Rho occurred when these mutants were expressed in rho$^{-/-}$ mice (Concepcion *et al.*, 2002; Concepcion and Chen, 2010); the lack of rod outer segments in these retinas, however, makes the trafficking effect of the mutations difficult to interpret.

An important finding from the present study was that the presence of the C-terminal VxPx sequence on the two GPCRs examined had essentially the opposite effect on ciliary enrichment in IMCD3 cells than it did for enrichment within the ciliary outer segment of rod photoreceptors. VxPx is required for proper outer segment enrichment of rhodopsin in rods, whereas in IMCD3, primary cilia VxPx significantly disrupt ciliary enrichment of both SR3 and Rho-i3S chimeras (Figure 7). Instead, dual Ax(S/A)xQ motifs within the i3 loops of SR3 or the Rho-i3S chimera were required for ciliary access and enrichment in IMCD3 cells (Figures 5 and 7 and Table 1), in agreement with a previous study (Berbari *et al.*, 2008). Of interest, the deletion of the C-terminal VxPx from Rho that possessed the native Rho i3 loop had no effect on its ciliary access (Table 1), suggesting that the VxPx motif, on its own, possess no ciliary enrichment or depletion activity in IMCD3 cells for either of the GPCRs we studied.

Taken together, the results presented here point to distinct pathways for enrichment of rhodopsin-like GPCRs in IMCD3 cell primary cilia and rod photoreceptor ciliary outer segments. Of importance, the VxPx motif, which is involved in post-Golgi sorting of rhodopsin in rod photoreceptors, a step required for proper outer segment rhodopsin delivery, does not appear to be required for delivery of these GPCRs to IMCD3 cell primary cilia. Instead. IMCD3 cells rely on an as-yet-unidentified sorting mechanism that requires the dual i3-loop Ax(S/A)xQ motifs with which the VxPx motif interferes. Thus the study of GPCR trafficking mechanisms in one cell type does not necessarily reveal the mechanisms used by another cell type.

Is there a role for VxPx in enriching GPCRs or other membrane proteins within primary cilia?

At first blush, our conclusions that VxPx disrupts ciliary enrichment of GPCRs containing the dual Ax(S/A)xQ sequences and has no effect on the distribution of GPCRs that lack them appear at variance with previous reports. Wang *et al.* (2012) and Trivedi *et al.* (2012) reported that expression of Rho-GFP-c8R from the same vector we used here, which contains a repeat of the VxPx motif after EGFP, is localized to the ciliary compartment of IMCD3 and hTERT-RPE1 cells. However, neither group investigated the role of VxPx on rhodopsin transport to the epithelial cell primary cilia. Moreover, neither group used quantitative approaches to examine ciliary enrichment. Examination of fluorescence micrographs in those reports revealed considerable levels of Rho-GFP-c8R in the apical membranes. Indeed, our direct analysis of images extracted from their work revealed F_{cil}/F_{am} ratios of 0.96 (Wang *et al.* (2012) and 1.5 (Trivedi *et al.* (2012), both of which are well below the enrichment threshold that we introduced here. We also found occasional detectable cilia in cells expressing Rho-GFP-c8R, particularly if the cilium extended over a neighboring cell that lacked expression or over a region absent of cells. However, the F_{cil}/F_{am} = 1.08 for Rho-GFP-c8R (Table 1) showed that the density in the ciliary membrane was lower on average than that in the apical membrane. Thus it appears that, upon quantification, the distributions of rhodopsin in the primary cilium-possessing epithelial cells used in all of these studies are in good agreement, showing that rhodopsin density is lower in the ciliary membrane than in the apical membrane and therefore is not enriched within the cilium.

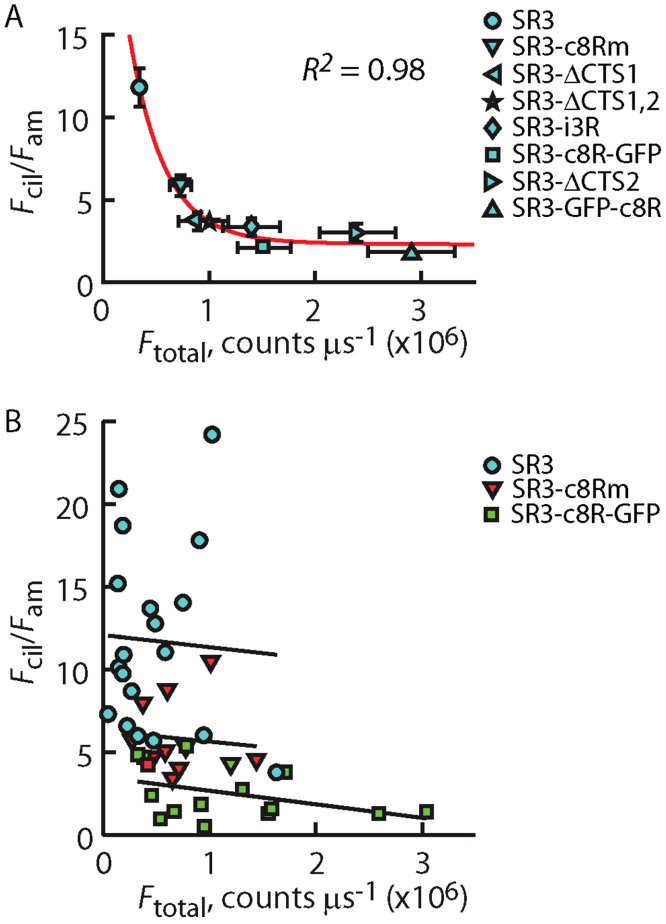

FIGURE 9: Ciliary enrichment correlates with average overall expression levels of different SR3 constructs but not with the variation in expression within a given construct. (A) Average F_{cil}/F_{am} of indicated SR3-GFP construct plotted against the average F_{total} for that construct. Vertical and horizontal error bars represent the SEM of the F_{cil}/F_{am} ratio and the F_{total} values, respectively. Red line represents fitting of the data by an exponential function. R^2 is a measure of goodness of fit. where a value of 1 indicating perfect fit. (B) Scatter of F_{cil}/F_{am} vs. F_{total} for individual cells of the indicate SR3-GFP constructs. Lines are linear regressions through each of the scatter plots, showing a lack of significant correlation between F_{cil}/F_{am} and F_{total} for any of the constructs. Data for SR3-GFP are reproduced from Figure 5E.

Our results do not exclude the possibility that the VxPx or related motifs are important for access or enrichment of other membrane proteins in primary cilia. For example, a C-terminal VxPx motif and the Arf4-mediated post-Golgi sorting machinery were implicated in the ciliary enrichment of polycystin-1 in human, mouse, and canine kidney epithelial cells (Ward *et al.*, 2011). Ward *et al.* (2011) quantified ciliary access by counting the proportion of ciliated cells that are visible upon antibody labeling for the protein construct of interest, an approach that does not differentiate cilium access from cilium enrichment. Close examination of their results, however, clearly shows significant fluorescence in the apical membranes adjacent to the cilia. It is thus unclear whether the polycystin-1 chimeras studied in Ward *et al.* (2011) were enriched in the cilia or merely had access to the ciliary compartment. Moreover, a later study showed that the deletion of the VxPx motif did not affect polycystin-1 localization in collecting duct epithelium cilia (Su *et al.*, 2015).

Distinction between ciliary access and ciliary enrichment of rhodopsin-like GPCRs: implications for enrichment mechanisms

The distinction between mere ciliary access and ciliary enrichment leads to significant questions about the molecular and physical mechanisms by which membrane proteins gain access to the ciliary compartment and are retained there and how the relative densities of the proteins within the contiguous ciliary and apical membranes are regulated. A hint about these mechanisms comes from the observation that ciliogenesis leads to marked, approximately threefold reduction in the overall expression of SR3-EGFP (Figure 8). This result shows that ciliary enrichment of SR3 is effected, in part, by large-scale retrieval of the GPCR from other membrane compartments upon ciliogenesis. Retrieval and degradation of GPCRs that have transported to membranes other than the ciliary membrane might therefore also play a role in maintaining their higher ciliary membrane density at the steady state, when ciliogenesis is complete. Indeed, the average level of ciliary enrichment of the SR3 chimeras that we examined scaled inversely with the average expression level, whereas the ciliary enrichment of the individual constructs did not (Figure 9 and Table 1), suggesting that reduced overall expression by receptor retrieval from nonciliary membrane compartments and their subsequent degradation is a key element of ciliary enrichment. Additional mechanisms resulting in reduced overall receptor expression with enhanced ciliary enrichment might be at play, including changes in transcription and/or translation, together with changes in transport target from the apical membrane toward a more direct line to the cilium upon ciliogenesis. Further study is needed to identify these important mechanisms.

Conclusion

We presented a novel approach to quantifying the enrichment of membrane proteins in primary cilia that accounts for the specific geometry of the membranes and the optical properties of the imaging system. Using this approach, we showed that, in cultured epithelial cells, a bright cilium does not necessarily connote ciliary enrichment of a fluorescently labeled membrane protein and that that ciliary enrichment of the somatostatin receptor 3 in IMCD3 cells is not likely achieved by any one mechanism. Ciliary enrichment of membrane proteins thus likely includes membrane and protein transport, sorting, retrieval, and degradation mechanisms acting in concert.

MATERIALS AND METHODS

DNA constructs and protein expression in IMCD3 cells

The somatostatin receptor 3-EGFP (SR3-EGFP) fusion construct was a gift from Kirk Mykytyn (Ohio State University, Columbus, OH). mKate2 was a gift from Erik Lee Snapp (Albert Einstein College of Medicine, New York, NY). The bovine rod opsin-EGFP construct, originally produced in the Oprian lab (Jin *et al.*, 2003) and obtained from David S. Williams (Jules Stein Eye Institute, University of California, Los Angeles, CA), consists of the full length of bovine opsin, followed by EGFP on the C-terminus and then the eight C-terminal amino acids of bovine opsin repeated after the EGFP. Although the opsin constructs would only be considered "rhodopsins" if the chromophore 11-*cis*-retinal were bound to them, we refer to the protein products here as rhodopsin, or Rho.

DNA constructs (Figure 1) were created using standard cloning and mutagenesis methods. A rhodopsin chimera with third intracellular loop of SR3 (T236–R258) replacing the third intracellular loop of rhodopsin (E232–K248), Rho-i3S, was constructed using the FastCloning method (Li *et al.*, 2011). The reverse was done for

the creation of the SR3-i3R-GFP chimera. The SR3-mKate2 fusion protein was created by subcloning mKate2 in place of EGFP in the SR3-EGFP construct. The SR3-ΔCTS1-GFP, SR3-ΔCTS2-GFP, and SR3-Δ-CTS1&2-GFP constructs were created by the deletion of CTS1, CTS2, and both CTS1 and 2, respectively, from the original SR3-EGFP. These and all other constructs with deletions or additions of short stretches of amino acids were produced using the QuikChange protocol. All constructs were verified by sequencing the entire coding region of the plasmid. Expression in IMCD3 kidney epithelial cells was driven by the CMV promoter, originally derived from pEGFPN1 (Clontech). Most plasmids were transiently transfected into IMCD3 cells that were growing on #1 coverslips (Fisher) using JetPrime (Polyplus) at concentration of 4 µg DNA/200 µl transfection buffer. To reduce the expression level of Rho-GFP and Rho-i3S-GFP, the plasmid concentration was reduced fivefold to 0.8 µg of DNA/200 µl of buffer.

Confocal microscopy

All imaging experiments were carried out using our custom confocal/multiphoton microscopy setup described previously (Peet *et al.*, 2004; Calvert *et al.*, 2007, 2010). Live IMCD3 cells expressing fluorescently tagged proteins were grown to confluency on #1 coverslips (Fisher) and then serum starved for 24–48 h to induce ciliogenesis. Coverslips were then placed in an imaging chamber, and the chamber was placed in a Peltier temperature controller on the microscope stage (Warner Instruments) and maintained at 37°C. Expressing cells and their cilia were located using epifluorescence visualization. Because the fluorescence from the ciliary membrane of cells expressing some of the rhodopsin variants was not sufficient to discriminate it from the background apical membrane fluorescence, we coexpressed SR3-mKate2, which served to mark the cilium in red. Confocal 3D scans with at most 0.1-µm frequency in *xy* and a *z*-step of 0.1 or 0.2 µm were obtained with the 488-nm line of an argon-ion laser (Newport) focused to the diffraction limit with a 60×/1.2 numerical aperture, water-immersion objective (Plan Apo VC; Nikon).

Direct measurement of the *psf* profile in our confocal microscope was performed by scanning 0.1-µm-diameter fluorescent microspheres and fitting the fluorescence profiles with Gaussians, as described previously (Peet *et al.*, 2004; Najafi *et al.*, 2012). This analysis yielded SDs in *xy* and *z* of $\sigma_{xy} = 0.14$ µm and $\sigma_z = 0.56$ µm, respectively. To determine the theoretical enrichment threshold (Figure 3), we approximated the *psf* intensity profile as a 3D Gaussian,

$$I_{psf}(x,y,z) = a\,\exp\left(-\frac{(x^2+y^2)}{2\sigma_{x.y}^2}\right)\exp\left(-\frac{z^2}{2\sigma_z^2}\right)$$

where *a* is the intensity maximum at the 3D center of the profile. For this analysis, we used a normalized *psf* profile, where $\iiint_{xyz} I_{psf} = 1$.

Image analysis was performed using custom Matlab programs. Analysis programs are available upon request.

Statistical analysis

We compared mean F_{cil}/F_{am} ratios or mean total expression of multiple different fluorescently labeled proteins. Thus, for each discrete set of comparisons, a one-way analysis of variance was performed with $\alpha = 0.05$, where the null hypothesis was that all mean values were equal. Upon rejection of the null hypothesis with $p < 0.05$, post hoc comparisons among the mean values were carried out by two-sample *t* test. To account for the variance among the multiple pairs of mean values compared, the Bonferroni correction was applied to α such that $\alpha_b = \alpha/m$, where α_b is the corrected α, and *m* is the number of comparisons being made among the means.

Correlation analysis was performed to explore possible dependences between F_{cil}/F_{am} and fusion protein expression level. Linear correlation was performed in Matlab using linear least squares regression. Pearson's product moment coefficients (*r*) were calculated to evaluate linear dependence. Coefficient of determination (R^2) values were used to determine goodness of fit. To evaluate the possibility of nonlinear correlations, Spearman's rank correlation analyses were performed to obtain Spearman's coefficient (ρ).

ACKNOWLEDGMENTS

We thank Rahul Angra for technical assistance. This work was supported by National Institutes of Health Grant RO1EY018421 (P.D.C.), a Postdoctoral Award from Fight for Sight (H.Y.T.), and an unrestricted grant to the SUNY Upstate Department of Ophthalmology from Research to Prevent Blindness.

REFERENCES

Berbari NF, Johnson AD, Lewis JS, Askwith CC, Mykytyn K (2008). Identification of ciliary localization sequences within the third intracellular loop of G protein-coupled receptors. Mol Biol Cell 19, 1540–1547.

Calvert PD, Peet JA, Bragin A, Schiesser WE, Pugh EN Jr (2007). Fluorescence relaxation in 3D from diffraction-limited sources of PAGFP or sinks of EGFP created by multiphoton photoconversion. J Microsc 225, 49–71.

Calvert PD, Schiesser WE, Pugh EN Jr (2010). Diffusion of a soluble protein, photoactivatable GFP, through a sensory cilium. J Gen Physiol 135, 173–196.

Concepcion F, Chen J (2010). Q344ter mutation causes mislocalization of rhodopsin molecules that are catalytically active: a mouse model of q344ter-induced retinal degeneration. PLoS One 5, e10904.

Concepcion F, Mendez A, Chen J (2002). The carboxyl-terminal domain is essential for rhodopsin transport in rod photoreceptors. Vision Res 42, 417–426.

Corbit KC, Aanstad P, Singla V, Norman AR, Stainier DY, Reiter JF (2005). Vertebrate smoothened functions at the primary cilium. Nature 437, 1018–1021.

Deretic D (2006). A role for rhodopsin in a signal transduction cascade that regulates membrane trafficking and photoreceptor polarity. Vision Res 46, 4427–4433.

Deretic D, Papermaster DS (1991). Polarized sorting of rhodopsin on post-Golgi membranes in frog retinal photoreceptor cells. J Cell Biol 113, 1281–1293.

Deretic D, Schmerl S, Hargrave PA, Arendt A, McDowell JH (1998). Regulation of sorting and post-Golgi trafficking of rhodopsin by its C-terminal sequence QVS(A)PA. Proc Natl Acad Sci USA 95, 10620–10625.

Deretic D, Wang J (2012). Molecular assemblies that control rhodopsin transport to the cilia. Vision Res 75, 5–10.

Dwyer ND, Adler CE, Crump JG, L'Etoile ND, Bargmann CI (2001). Polarized dendritic transport and the AP-1 mu1 clathrin adaptor UNC-101 localize odorant receptors to olfactory cilia. Neuron 31, 277–287.

Emmer BT, Maric D, Engman DM (2010). Molecular mechanisms of protein and lipid targeting to ciliary membranes. J Cell Sci 123, 529–536.

Follit JA, Li L, Vucica Y, Pazour GJ (2010). The cytoplasmic tail of fibrocystin contains a ciliary targeting sequence. J Cell Biol 188, 21–28.

Geng L, Okuhara D, Yu Z, Tian X, Cai Y, Shibazaki S, Somlo S (2006). Polycystin-2 traffics to cilia independently of polycystin-1 by using an N-terminal RVxP motif. J Cell Sci 119, 1383–1395.

Godsel LM, Engman DM (1999). Flagellar protein localization mediated by a calcium-myristoyl/palmitoyl switch mechanism. EMBO J 18, 2057–2065.

Hu Q, Milenkovic L, Jin H, Scott MP, Nachury MV, Spiliotis ET, Nelson WJ (2010). A septin diffusion barrier at the base of the primary cilium maintains ciliary membrane protein distribution. Science 329, 436–439.

Jenkins PM, Hurd TW, Zhang L, McEwen DP, Brown RL, Margolis B, Verhey KJ, Martens JR (2006). Ciliary targeting of olfactory CNG channels requires the CNGB1b subunit and the kinesin-2 motor protein, KIF17. Curr Biol 16, 1211–1216.

Jin S, McKee TD, Oprian DD (2003). An improved rhodopsin/EGFP fusion protein for use in the generation of transgenic Xenopus laevis. FEBS Lett 542, 142–146.
Laird JG, Pan Y, Modestou M, Yamaguchi DM, Song H, Sokolov M, Baker SA (2015). Identification of a VxP targeting signal in the flagellar Na(+)/K(+) -ATPase. Traffic 16, 1239–1253.
Li C, Wen A, Shen B, Lu J, Huang Y, Chang Y (2011). Fastcloning: a highly simplified, purification-free, sequence- and ligation-independent PCR cloning method. BMC Biotechnol 11, 92.
Lodowski KH, Lee R, Ropelewski P, Nemet I, Tian G, Imanishi Y (2013). Signals governing the trafficking and mistrafficking of a ciliary GPCR, rhodopsin. J Neurosci 33, 13621–13638.
Luo W, Marsh-Armstrong N, Rattner A, Nathans J (2004). An outer segment localization signal at the C terminus of the photoreceptor-specific retinol dehydrogenase. J Neurosci 24, 2623–2632.
Marshall WF, Nonaka S (2006). Cilia: tuning in to the cell's antenna. Curr Biol 16, R604–R614.
Mazelova J, Astuto-Gribble L, Inoue H, Tam BM, Schonteich E, Prekeris R, Moritz OL, Randazzo PA, Deretic D (2009). Ciliary targeting motif VxPx directs assembly of a trafficking module through Arf4. EMBO J 28, 183–192.
Najafi M, Haeri M, Knox BE, Schiesser WE, Calvert PD (2012). Impact of signaling microcompartment geometry on GPCR dynamics in live retinal photoreceptors. J Gen Physiol 140, 249–266.
Pazour GJ, Witman GB (2003). The vertebrate primary cilium is a sensory organelle. Curr Opin Cell Biol 15, 105–110.
Peet JA, Bragin A, Calvert PD, Nikonov SS, Mani S, Zhao X, Besharse JC, Pierce EA, Knox BE, Pugh EN Jr (2004). Quantification of the cytoplasmic spaces of living cells with EGFP reveals arrestin-EGFP to be in disequilibrium in dark adapted rod photoreceptors. J Cell Sci 117, 3049–3059.
Singla V, Reiter JF (2006). The primary cilium as the cell's antenna: signaling at a sensory organelle. Science 313, 629–633.
Su X, Wu M, Yao G, El-Jouni W, Luo C, Tabari A, Zhou J (2015). Regulation of polycystin-1 ciliary trafficking by motifs at its C-terminus and polycystin-2 but not by cleavage at the GPS site. J Cell Sci 128, 4063–4073.
Tai AW, Chuang JZ, Bode C, Wolfrum U, Sung CH (1999). Rhodopsin's carboxy-terminal cytoplasmic tail acts as a membrane receptor for cytoplasmic dynein by binding to the dynein light chain Tctex-1. Cell 97, 877–887.
Tam BM, Moritz OL, Hurd LB, Papermaster DS (2000). Identification of an outer segment targeting signal in the cooh terminus of rhodopsin using transgenic Xenopus laevis. J Cell Biol 151, 1369–1380.
Trivedi D, Colin E, Louie CM, Williams DS (2012). Live-cell imaging evidence for the ciliary transport of rod photoreceptor opsin by heterotrimeric kinesin-2. J Neurosci 32, 10587–10593.
Wang J, Deretic D (2014). Molecular complexes that direct rhodopsin transport to primary cilia. Progress Retinal Eye Res 38, 1–19.
Wang J, Morita Y, Mazelova J, Deretic D (2012). The Arf GAP ASAP1 provides a platform to regulate Arf4- and Rab11-Rab8-mediated ciliary receptor targeting. EMBO J 31, 4057–4071.
Ward HH, Brown-Glaberman U, Wang J, Morita Y, Alper SL, Bedrick EJ, Gattone VH 2nd, Deretic D, Wandinger-Ness A (2011). A conserved signal and gtpase complex are required for the ciliary transport of polycystin-1. Mol Biol Cell 22, 3289–3305.